Stratigraphic Reconnaissance of the Helderberg Group near Moorefield, West Virginia

Nicholas Baumann
GEOL394
4/25/16

Advisors: Dr. Alan J. Kaufman
Dr. John Merck

Abstract

Lithologic and chemical stratigraphy were measured at limestone outcrops of the Helderberg Group near Moorefield, West Virginia. Silicified limestone was observed instead of the siltstone of the Shriver Chert. This and an interfingering relationship between the Shriver Chert and the Oriskany Sandstone reflect a shallower depositional environment for the Shriver Chert. The large carbon isotope anomaly known globally as the Klonk event at the Silurian-Devonian boundary was identified. The isotopic composition of pyritic sulfur and organic carbon were measured for the first time across the Silurian-Devonian boundary. A positive excursion in pyritic sulfur isotope values is not coupled with the negative excursion in sulfate sulfur isotope values previously measured in the Helderberg Group. This probably reflects stratified conditions at the ocean bottom restricting replenishment of sulfate during sulfate reduction. Organic carbon isotope values are roughly constant, not coupled with bulk carbon. This could be caused by a large influx of organic carbon into the system, lessening the effect of the isotopic shift of bulk carbon on the organic carbon. These findings support the hypothesis that the Silurian-Devonian boundary coincides with an interval of increased weathering and ocean stratification.

Table of Contents

List of Figures

List of Tables

Introduction

The Silurian-Devonian boundary, 419 million years ago (Cohen et al., 2013), is well known from Hutton's unconformity, but events at that time are not particularly well-understood. It is not marked by a major mass extinction like many other period boundaries of the Phanerozoic. However, there has long been evidence for a local extinction in Europe, and there is increasing evidence that there was a minor global extinction event (Jeppsson, 1998). This is known as the Klonk event, after the type section of the Silurian-Devonian boundary in the Czech Republic. It is mainly known for affecting graptolites and conodonts, but it also affected chitinozoans, trilobites, ostracods, cephalopods, bivalves, and brachiopods.

The Klonk event is also noticeable in the geochemical record of marine strata. The Silurian-Devonian boundary marks the peak in ^{87}Sr/^{86}Sr of marine proxies, which had been increasing from 0.7078 at the beginning of the Silurian Period (Figure 1; Burke et al., 1982). Radioactive decay of ^{87}Rb from weathered igneous continental rocks is the main source of ^{87}Sr in the oceans, so a higher proportion of ^{87}Sr could indicate increased weathering at that time (Burke et al., 1982; Kaufman et al., 1993). The Silurian-Devonian boundary also coincides with a global positive carbon isotope excursion of over +4‰; one of the largest carbon cycle anomalies of the Paleozoic (Figure 2). This event has been detected at multiple locations in North America and Europe, and one location in Australia (Malkowski and Racki, 2009).

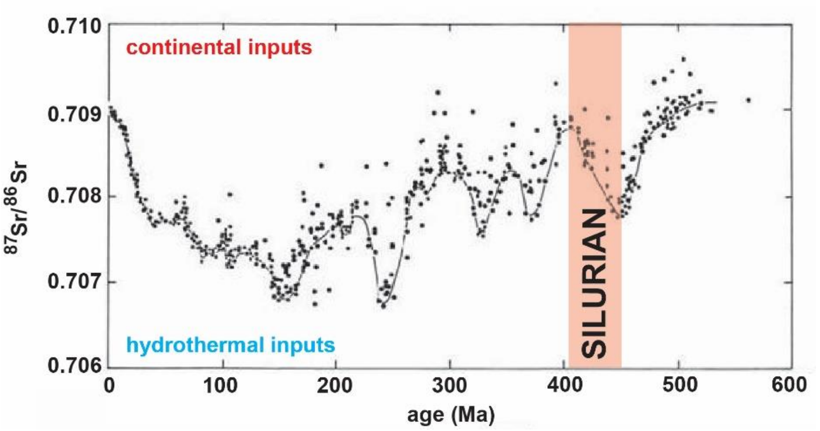

Figure 1: ^{87}Sr/^{86}Sr variations over Phanerozoic time, with the significant rise from 0.7080 to 0.7090 in the Silurian Period highlighted (Modified from Burke et al., 1982).

The carbon isotope compositions of seawater proxies can be influenced by several factors, but the most likely driving factor is usually organic carbon burial. Lighter ^{12}C is preferentially taken up by photosynthetic primary producers, so burial of dead phytoplankton and organisms that consume them would remove lighter carbon from the system and increase the proportion of ^{13}C dissolved in seawater, available for carbonate formation. On the other hand, weathering of fossil organic matter during sea level fall could then release ^{12}C back into the system. The carbon isotope compositions of seawater proxies can also be influenced by a change in the isotopic signature of weathered products, a change in the biological fractionation process, or diagenesis (Magaritz et al., 1992). An increase in the burial of organic carbon would agree with the increased weathering indicated by strontium isotopes insofar as weathering would also deliver nutrients to the oceans, thereby stimulating photosynthesis. On the other hand, another proposed explanation for the excursion at the Silurian-Devonian boundary is that regression exposed ocean sediments that were previously enriched in ^{13}C, which were subsequently weathered. This change in the isotopic composition of carbon input into the system may alternatively have driven the excursion (Saltzman, 2002).

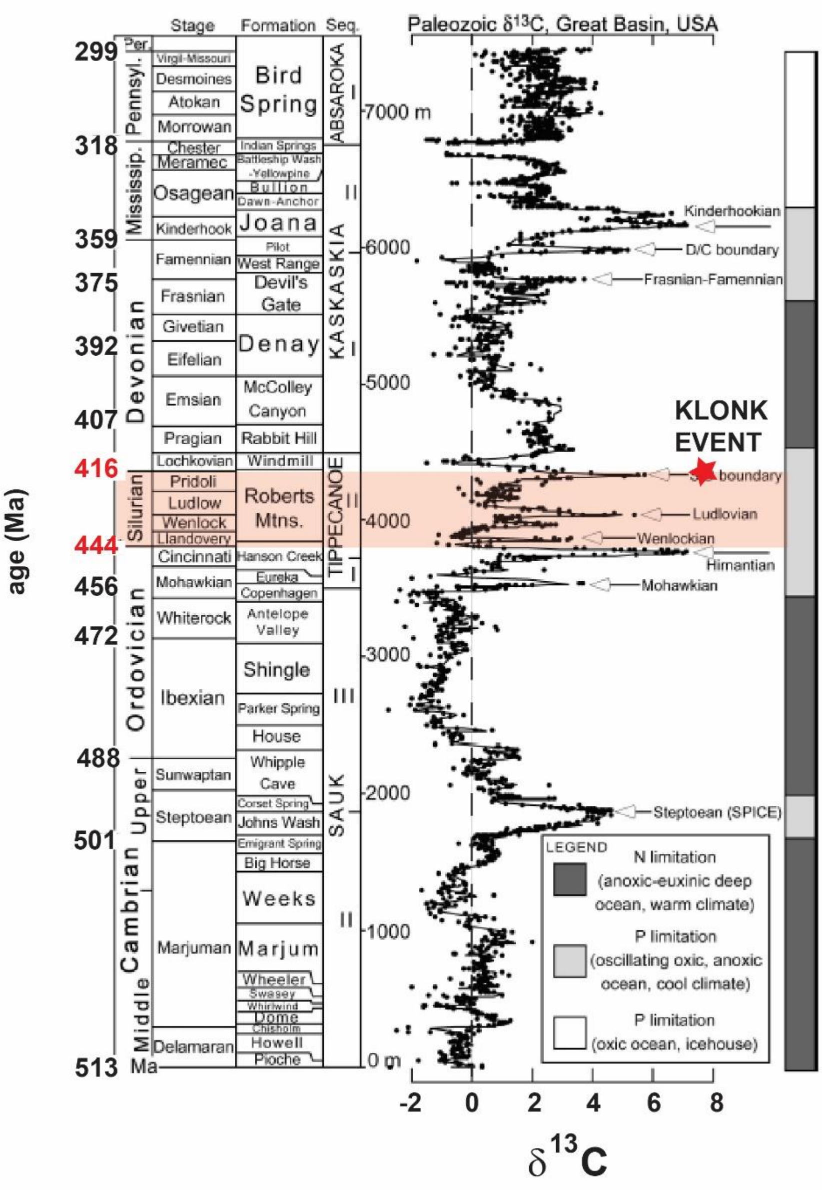

Figure 2: Paleozoic carbon isotope variations recorded in the Great Basin, USA. The time-series trend shows that the Silurian (highlighted in tan) characterizes the most unstable interval, and ends with a positive δ^{13}C anomaly (the Klonk Event), which is preserved in the Helderberg Group of West Virginia (Modified from Saltzman et al., 2005).

The sulfur isotopic composition of seawater proxies may also provide clues for understanding the carbon isotope anomaly. Sulfur in the ocean mainly comes from sulfate weathered from the continents (Gill et al., 2007). In anoxic waters, the process of microbial sulfate reduction consumes sulfate and creates hydrogen sulfide that will combine with ferrous iron to form pyrite. This process favors lighter ^{32}S over ^{34}S, leading to progressive increases in δ^{34}S of residual sulfate as pyrite is buried. The most likely explanation for higher δ^{34}S values of carbonate associated sulfate (CAS) in the stratigraphic record is thus increased pyrite burial (Gill et al., 2007). However, a change in δ^{34}S values can also be caused by a change in the isotopic composition of sulfate input into the ocean, or a change in the fractionation process (Hammarlund et al., 2012). Increased burial of organic carbon and pyrite often occur together, leading to coupled excursions of carbon and sulfur isotopes.

In the central Appalachians, the Silurian-Devonian boundary occurs within the Helderberg Group, a series of limestones deposited in a shallow, passive margin setting (Dorobek and Read, 1986). It extends from southeast West Virginia and neighboring Virginia through Maryland and Pennsylvania to central New York (Dorobek and Read, 1986). In 2010, the state of West Virginia opened a new section of highway containing road cuts through the Helderberg Group. This road, called Corridor H, has been under construction across northeast West Virginia since 2000 (West Virginia Division of Highways). I have studied an outcrop of the Helderberg Group along Corridor

H near Moorefield, West Virginia with the goal of learning more about regional stratigraphy and the geochemistry of the Silurian-Devonian boundary. In particular, I aimed to find evidence of the Klonk event and obtain new information that may provide possible explanations for the carbon isotope anomaly.

Regional Geologic Background

Lithostratigraphy

The Helderberg Group was deposited along a passive continental margin after the Taconic orogeny ended ~440 million years ago (Dorobek and Read, 1986). During the Silurian and Devonian periods, the foreland basin created during mountain-building gradually filled with sediment. That interval was subsequently interrupted by the Acadian orogeny, ~375 million years ago.

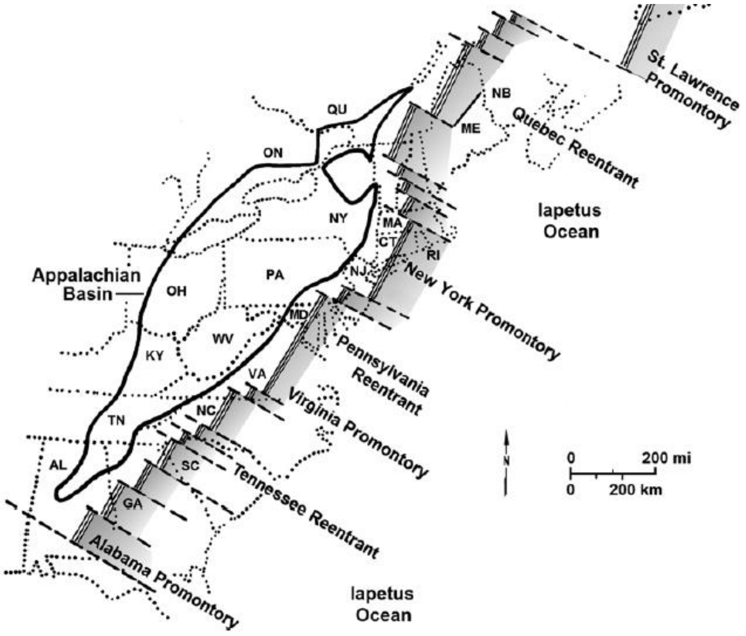

Figure 3: The Helderberg Group was deposited in the central eastern part of the Appalachian Basin, shown here along with the possible positions of transform faults, from Ettensohn and Lierman (2015)

The Helderberg Group consists of the shallow ramp of carbonate sediments leading up towards the central eastern shore of that basin (Figure 3). The facies of those sediments changed over time as fluctuations in sea level affected their depth. The subdivisions of the Helderberg Group in the central Appalachians are seen in Figure 4. My main source of information on the lithostratigraphy of the Helderberg Group in the area of the study location is Dorobek and Read (1986).

At the base of the Helderberg Group is the Keyser Limestone, by far the thickest formation of the succession. The lower part of the Keyser Limestone was deposited when the basin was fairly deep. It tends to be argillaceous because it was so deep that the carbonate sediment mixed with some siliciclastic mud. It is also nodular when weathered (Head, 1969). The Keyser Limestone is subdivided by the Big Mountain Shale. As sea level rose, the basin filled mainly with siliciclastic mud. The shale is olive green and calcareous. In the vicinity of the study location, the Big Mountain Shale is a few meters thick. Immediately above the Big Mountain Shale, the Keyser Limestone consists of packstone, which is a grain supported limestone with a lime mud matrix. The grains consist of fine to medium-sized skeletal and pellet material, which is abraded and poorly sorted. This was deposited in water that was shallow, but still subtidal. The large grains and poor sorting of the packstone indicates that its components cannot be far from their source.

Figure 4: Stratigraphic subdivision of the Late Silurian Helderberg Group, including the Keyser, New Creek, and Corriganville limestones and the Shriver Chert (From Dorobeck and Read, 1986).

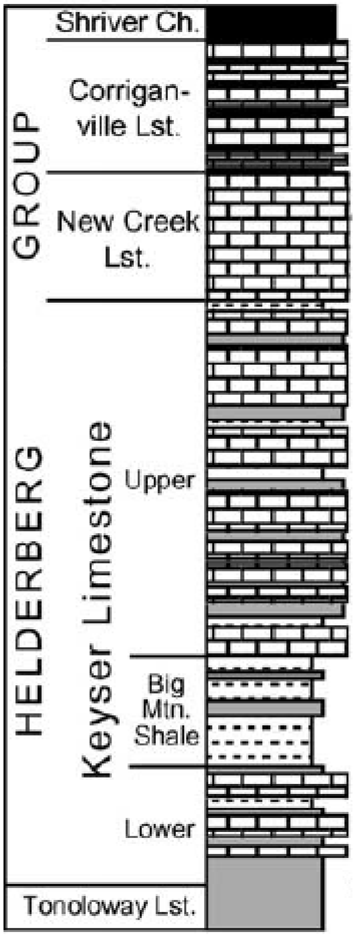

The top of the Keyser Limestone is a mix of the nodular, argillaceous limestone found at the bottom and different facies. This is not nodular, but contains some small shale layers, some pelletal packstone layers, and some skeletal sand lags. This interval of the Keyser Formation was deposited as sea level fluctuated, leading to changes between the deep facies seen lower down and the medium and shallower depth facies. Storms stirring up sediment probably caused the shale layers in that limestone. Depth shallowed towards the top of the Keyser Limestone, so that crossbedding indicative of a subtidal environment is observed in some locations (Gill et al., 2007).

Above the Keyser Limestone is the New Creek Limestone, a poorly sorted packstone with a larger grain size and a lighter color. It is notable for its abundance of brachiopod and crinoid fossils (Head, 1969). It seems to have been deposited in a shallow, subtidal environment, like the top of the Keyser Limestone. The New Creek Limestone is overlain by the Corriganville Limestone, which formed in deeper water. It is poorly sorted, with grains ranging from sand to mud size. It is notable for its light grey nodular chert, which is abundant throughout, but is increasingly abundant upwards (Head, 1969). The silica for the chert probably came from sponge spicules.

The Shriver Chert is a transition between the rest of the Helderberg Group and the overlying Oriskany Sandstone. The Shriver Chert consists mainly of dark shale and dark calcareous siltstone, with some limestone intervals. Aside from the limestone, it is increasingly calcareous upwards. It is notable for black chert, which is abundant throughout, but increasingly abundant downwards (Head, 1969). Finally, above the Helderberg Group and the Shriver Chert is the Oriskany Sandstone. It is easily recognizable as a very mature sandstone with abundant brachiopod casts. As a mature sandstone, it is very pure and light-colored, with well-rounded grains. It is overlain by the Needmore Shale in the region of this study (Dennison, 1961).

The Silurian-Devonian Boundary

The Silurian-Devonian boundary in the Helderberg Group has been determined from conodont biostratigraphy. At Strait Creek, Virginia (about 60 miles southwest of Moorefield), the Silurian-Devonian boundary was determined to be at least three meters below the top of the Keyser Limestone. Near Tyrone, Pennsylvania (about 110 miles northeast of Moorefield), the boundary was determined to be less than 20 meters below the top of the Keyser Limestone (Denkler and Harris, 1988).

In recent decades, attention has shifted to the stable isotope geochemistry of the Helderberg Group as researchers realized that the carbon isotope anomaly at the Silurian-Devonian boundary may provide a global correlation marker. They also wanted to understand the environmental or biological processes behind major carbon cycle anomalies. At Smoke Hole, West Virginia (about 30 miles southwest of Moorefield), $\delta^{13}C$ values were shown to increase across about 50 meters of section from 0‰ at the bottom of the Helderberg Group to a peak of +5‰ at the Silurian-Devonian boundary (Figure 5). Then, $\delta^{13}C$ values decreased back down to 0‰ at the top of the Helderberg Group across another 50 meters of section (Saltzman, 2002). $\delta^{18}O$ values of the Smoke Hole carbonates increase up section from about -8‰ at the base of the succession to about -6‰ near the Silurian-Devonian boundary.

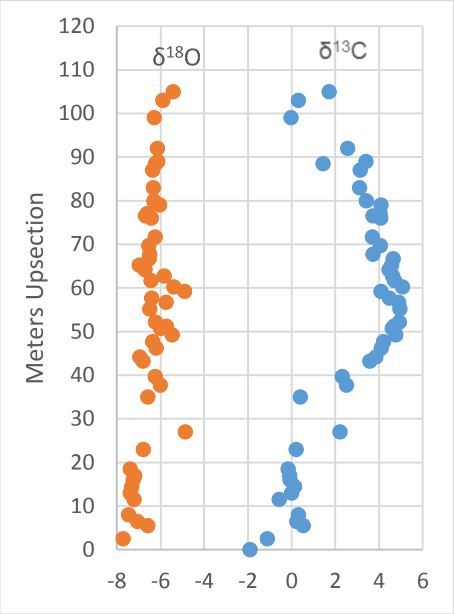

Figure 5: Carbon and oxygen isotope stratigraphy of the Helderberg Group at Smoke Hole, West Virginia (data from Saltzman, 2002).

Researchers also measured the isotopic composition of sulfur from Carbonate Associated Sulfate (or CAS) in the Helderberg Group (Gill et al., 2007). At Strait Creek, CAS in the limestone has a low $\delta^{34}S$ value of +11‰ coincident with the carbon isotope peak (Figure 6). This occurs in an interval starting a few meters below the top of the Keyser Limestone and extending downwards for about 25 meters, where $\delta^{34}S$ values are more variable and mostly between +20‰ and +25‰. Extending upwards for 25 meters from the top of the Keyser Limestone to the top of the Corriganville Limestone is another interval where $\delta^{34}S$ values are less variable and stay between +25‰ and +30‰. Notably, the negative excursion does not match the positive carbon isotope excursion. This observation seems to support the idea of a changed isotopic composition of inputs into the system. Isotopically light pyrite could have been exposed and weathered under an oxidizing atmosphere, leading to a delivery of ^{32}S enriched sulfate to the ocean and a subsequent negative excursion in CAS sulfur isotopes. Comparing the sulfur isotopes from sulfate with sulfur isotopes from pyrite could provide independent evidence for the process resulting in this anomaly. If they match, it would support the traditional idea of pyrite burial controlling $\delta^{34}S$ of CAS, but if they are not coupled, it would signify that another process was responsible (Hammarlund et al., 2012).

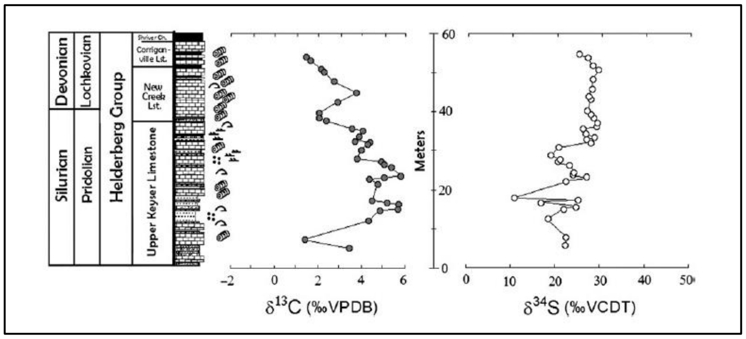

Figure 6: Carbon and CAS sulfur isotopic composition of Helderberg Group carbonates at Strait Creek, Virginia (From Gill et al., 2007).

Microbial sulfate reduction also relies on organic carbon, so pyrite burial is usually associated with organic carbon burial. Relative amounts of organic carbon and pyrite can reveal the degree of anoxia when the sediments were deposited (Berner and Raiswell, 1983). Organic carbon can also be compared against bulk carbon the same way sulfate and pyrite are compared. Parallel trends would support the idea of carbon burial, but different trends would suggest a different process.

Methods

Field

First, measurements were made of the outcrop in the field. A Jacobs staff was used to measure the distances between beds, and the locations of changes in lithology and other interesting textural features in relation to an initial datum (Figure 7). Measurements were made perpendicular to bedding in order to find the actual thicknesses of rocks rather than the distance along the outcrop surface. The datum was easy to identify so that it could be located on repeated trips to the outcrop and at different places on the outcrop. It was also thin and parallel to the other beds in order to be useful for measurement.

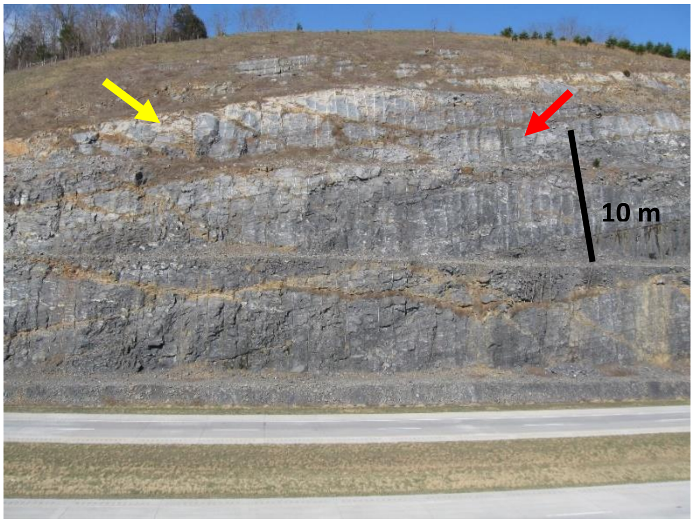

Figure 7: Photo of the southwest exposure of the outcrop at Location #1. The datum is indicated by the red arrow, and the position of the Oriskany Sandstone indicated by the yellow arrow.

The uncertainty of the measurement of the outcrop was determined by measuring one distance five times (Table 1). The standard deviation of the measurements was 0.3 meters, and the uncertainty is two standard deviations of the measurements, which is 0.6 meters. Along with these measurements, many other observations were recorded. Many pictures of the outcrop and of interesting features in the outcrop were taken, each including a scale for reference. Finally, hand samples were collected every one to two meters to bring back to the lab for geochemical analysis. These were carefully observed in the field under a hand lens and described. They were also tested with 3% hydrochloric acid, and the results of that test were recorded.

Distance from Datum to Shale Recorded at 5.7 m	
1st Measurement	5.7 m
2nd Measurement	5.2 m
3rd Measurement	5.8 m
4th Measurement	5.2 m
5th Measurement	5.7 m
Average	5.5 m
Standard Deviation	0.3 m
2 Standard Deviations	0.6 m

Table 1: Determination of uncertainty for field measurements

At the original study location (Location #1; 39° 7' N, 78° 59' W), most samples were collected on the southwest side of the road (Figures 7 and 8) and are numbered counting down section. Samples labeled "a" and were collected on the northeast side of the road, and are numbered counting up section. The sections measured on both sides of the road overlap for between seven and ten meters. Some hand samples collected in the field were too silicified for their isotopic compositions to be measured. Although Location #1 was the primary focus of this study, I also made use of a second outcrop, labeled Location #2 in Figure 8. It is about 2.4 miles northwest of Location #1. A regional geologic map tells me that Location #2 is closer to the axis of a large-scale anticline, so it must be down section of Location #1. In order to limit the scope of this project, only sample positions were measured at Location #2.

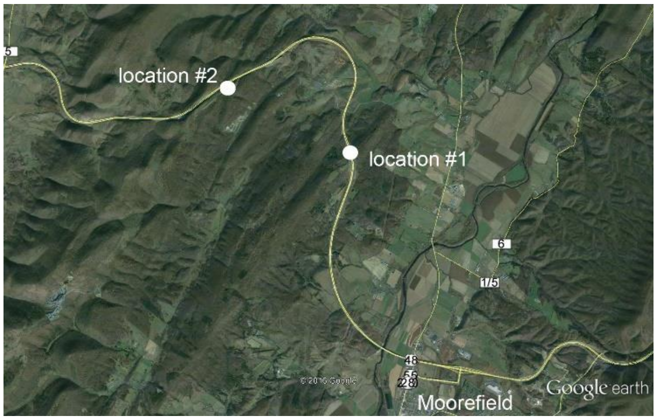

Figure 8: Locations of the two road cuts through the Helderberg Group studied along Corridor H northwest of Moorefield, WV.

Laboratory

At the laboratory, a water-cooled saw was used to cut a slab with roughly parallel sides out of each hand sample. Then, one side of each of those slabs was polished on a Struers LaboPol-21 polisher. These steps were necessary to prepare the samples for microdrilling (Figure 9). The drill requires a flat, smooth face in order to avoid unnecessary strain and wear. Before drilling, the samples were photographed because the polish may reveal previously unnoticed features. They were also observed and photographed under a microscope. Next, the samples were microdrilled to obtain powder for geochemical analysis. Several shallow drill holes were made in a small area of the sample with a 0.8 mm diameter carbide bit. Powder can also be obtained by crushing bulk samples of rock, but this method is not as precise. Drilling allows a researcher to pinpoint visually homogenous areas of rock, which are more likely to be isotopically homogenous as well. I tested multiple areas of some of my samples, but included comparable areas on all of them.

Figure 9: Servo Products drill in CHEM 0224 used to obtain powder for carbon and oxygen isotope analysis.

Next, 100 µg ± 10 µg of powder from each drill site was measured and put in an Exetainer vial. Several vials of the same amount of the JTB-1 standard were also prepared. These vials, along with some empty ones, were put in the MultiFlow peripheral analyzer (Figure 10) in-line with an Isoprime gas mass spectrometer. There, the air in the vials was flushed with helium because the carbon dioxide in the air would otherwise influence the results. After that, excess 100% phosphoric acid was added by syringe through a rubber septum, and allowed to react for one hour at 65 ºC. This released the carbon and oxygen of the carbonate rocks into a gas without adding water, which includes oxygen. Each exetainer's gas was individually removed on its way to the mass spectrometer. First, it passed through a Nafion water trap to remove any remaining water. Next, the different gases present passed through a gas chromatograph at different speeds, separating the carbon dioxide from any other gases. This way, the carbon and oxygen isotopes of the carbon dioxide could be measured alone. Finally, the carbon dioxide passed on to the mass spectrometer.

Figure 10: The MultiFlow analyzer in CHEM 1212 takes head space gas from acidifications of carbonate minerals to the Isoprime gas source mass spectrometer.

Meanwhile, samples for sulfur and organic carbon analysis were crushed prior to acidification to remove carbonate. A 3M hydrochloric acid solution was added to the powder until all the carbonate had dissolved. The carbon in the carbonate was removed as carbon dioxide, so only organic carbon and pyrite remained. The residue was then washed, and dried in an oven overnight. A few milligrams of powder from each sample was weighed out and put in tin capsules. For measuring sulfur, excess V_2O_5 was included to help the sample combust, but separate capsules without V_2O_5 were prepared for measuring organic carbon. Similar tin capsules with the NBS-127 and S-1 standards were also prepared for sulfur, and capsules with the urea standard were prepared for organic carbon.

These capsules were individually dropped into a Eurovector Elemental Analyzer in-line with a second Isoprime gas source mass spectrometer. There, they entered a 1030 ºC oven together with oxygen, allowing their contents to combust. Gaseous oxides of all the capsule's elements then formed. The excess oxygen reacted with copper, creating solid copper oxide. Those gaseous oxides then passed through a magnesium perchlorate water trap and a gas chromatograph prior to entering the source of the mass spectrometer.

The Mass Spectrometer

The mass spectrometer works the same in principle for all elements. Gas enters and is bombarded with electrons in order to ionize it. Those ions are accelerated along a path, but then encounter a magnetic field, changing their direction. Heavier ions are affected less by the magnetic field because they have more momentum. The final position of ions is measured, showing how much the magnetic field caused them to deviate from their original path. This therefore reveals their masses. Each sample run in the mass spectrometer is compared with a reference gas. The empty vials are run at the beginning and end of each set of bulk carbon and oxygen samples, also for reference.

Isotopic Uncertainties

Uncertainty of lab measurements is determined from measuring the standard deviation of the standards run along with the samples (Table 2). Maximum uncertainties were 0.07‰ for carbon, 0.15‰ for oxygen, 0.42‰ for sulfur, and 0.16‰ for organic carbon.

	$\delta^{18}O$	$\delta^{13}C$	$\delta^{13}C_{org}$	$\delta^{34}S$
Standard #1	-8.69‰	1.75‰	-29.36‰	20.60‰
Standard #2	-8.66‰	1.81‰	-29.30‰	21.15‰
Standard #3	-8.67‰	1.75‰	-29.34‰	21.11‰
Standard #4	-8.71‰	1.80‰	-29.56‰	20.86‰
Standard #5	-8.81‰	1.85‰	-29.35‰	21.41‰
Standard #6	-8.83‰	1.77‰	-29.43‰	20.96‰
Standard #7	-8.61‰	1.74‰	-29.43‰	
Standard #8	-8.70‰	1.78‰	-29.35‰	
Average	-8.71‰	1.78‰	-29.39‰	21.10‰
Standard Deviation	0.08‰	0.04‰	0.08‰	0.21‰
2 Standard Deviations	0.15‰	0.07‰	0.16‰	0.42‰

Table 2: Measurements of standard materials to determine uncertainties of isotope compositions for unknowns. The standard for carbon and oxygen in carbonate was JTB-1, for carbon in organic matter was urea, and for sulfur in pyrite was NBS-127 and NZ-1.

Results

Field observations reveal that near the top of the measured section is the Oriskany Formation, a mature sandstone with abundant brachiopod casts that is an important regional marker bed (Figure 7). Several meters of this sandstone lies between limestones, which are similar to each other. Below the sandstone the limestone is significantly silicified, and most-likely part of the Shriver Chert. Notably, the limestone above the Oriskany Sandstone was less silicified. The silicified limestone is nodular near the top of the section. Fossils are abundant throughout most of the silicified carbonates, with most being brachiopods. I also found a few tabulate and rugose corals. All the fossils are highly recrystallized (Figure 11a). Black chert is abundant towards the bottom of the section, but is absent in the upper part (Figure 11b).

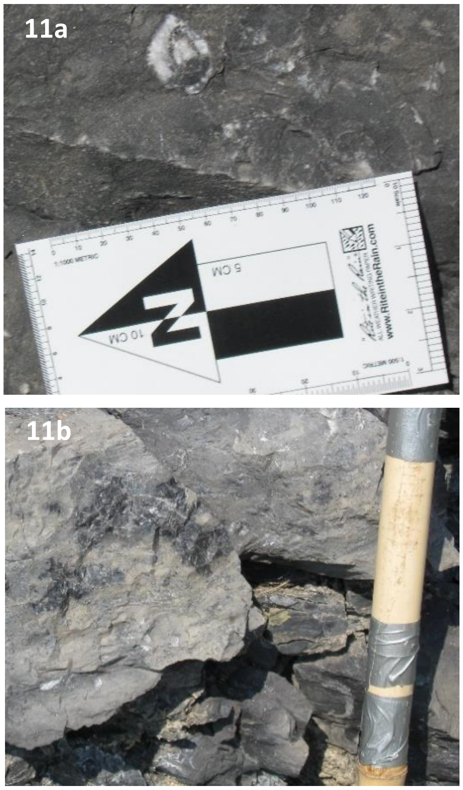

Figure 11: Field photos of recrystallized brachiopods (a) and black chert nodules (b) in the Shriver Chert beneath the Oriskany Sandstone along Corridor H.

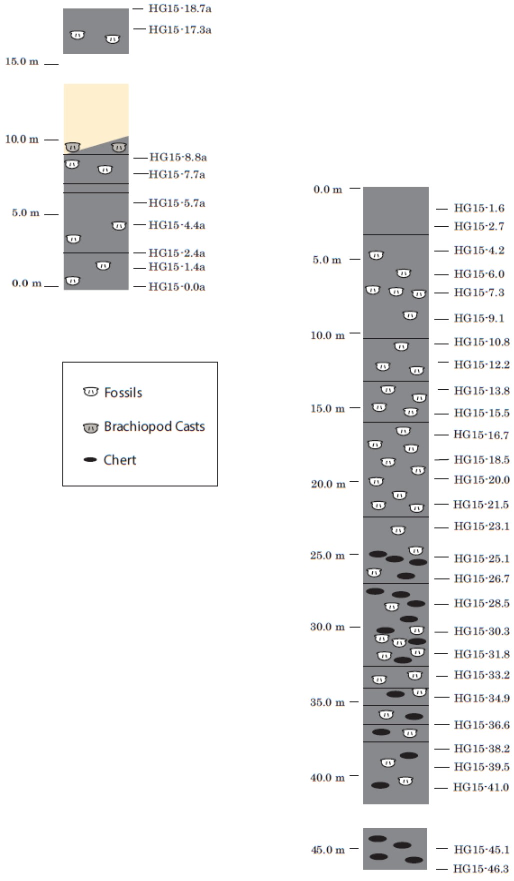

Descriptions of samples collected from Location #1 with Dunham classifications are presented in Appendix 1. The representative stratigraphic columns for this location with the position of collected samples is shown in Figure 12.

Figure 12: Stratigraphic column of top of the Helderberg Group (Shriver Chert below the Oriskany Sandstone) at Location #1, near Moorefield, West Virginia

Geochemical data from samples from Location #1 are reported in Appendix 2 and shown in Figure 13.

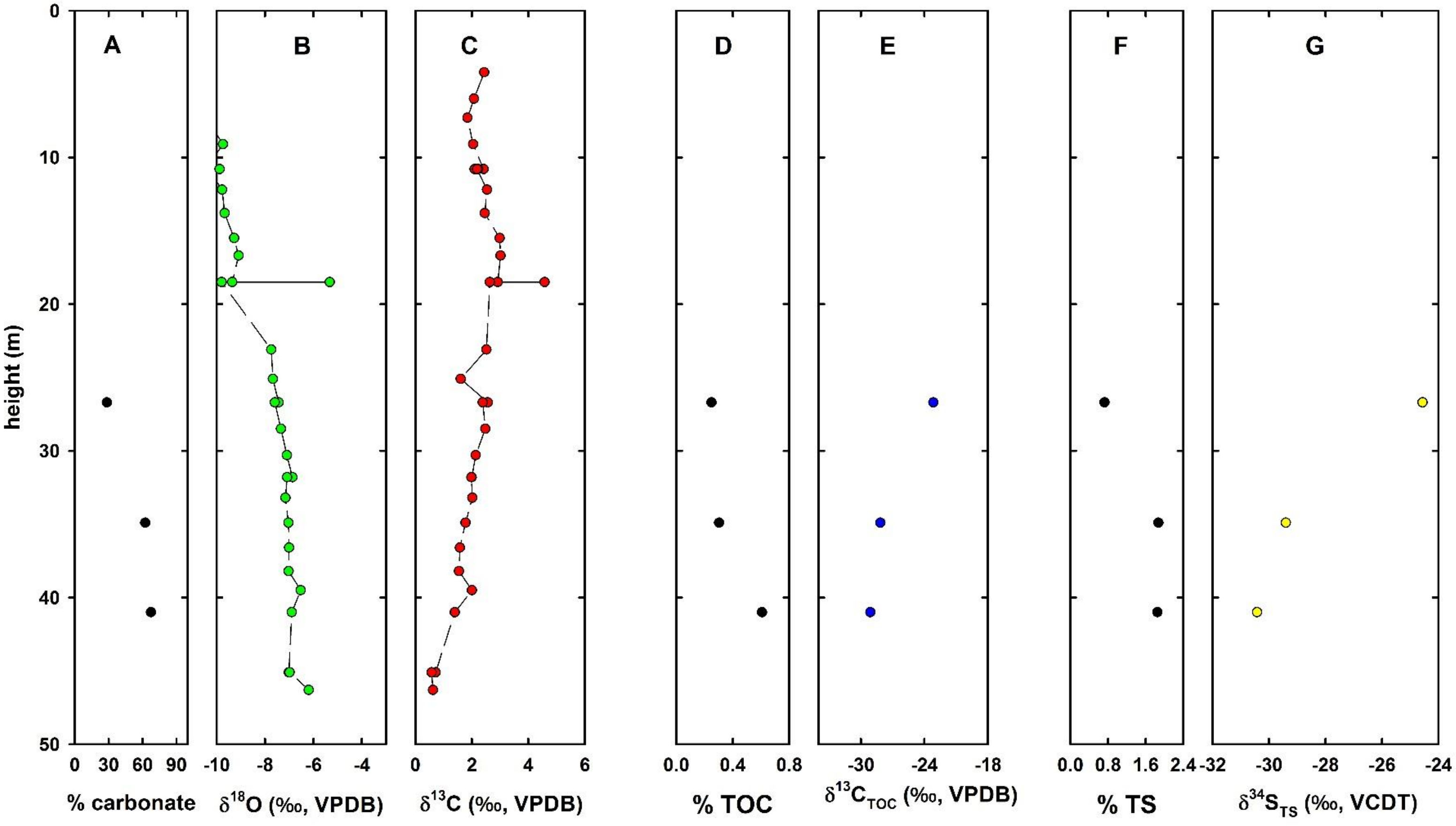

Figure 13: Geochemical Data from Location #1

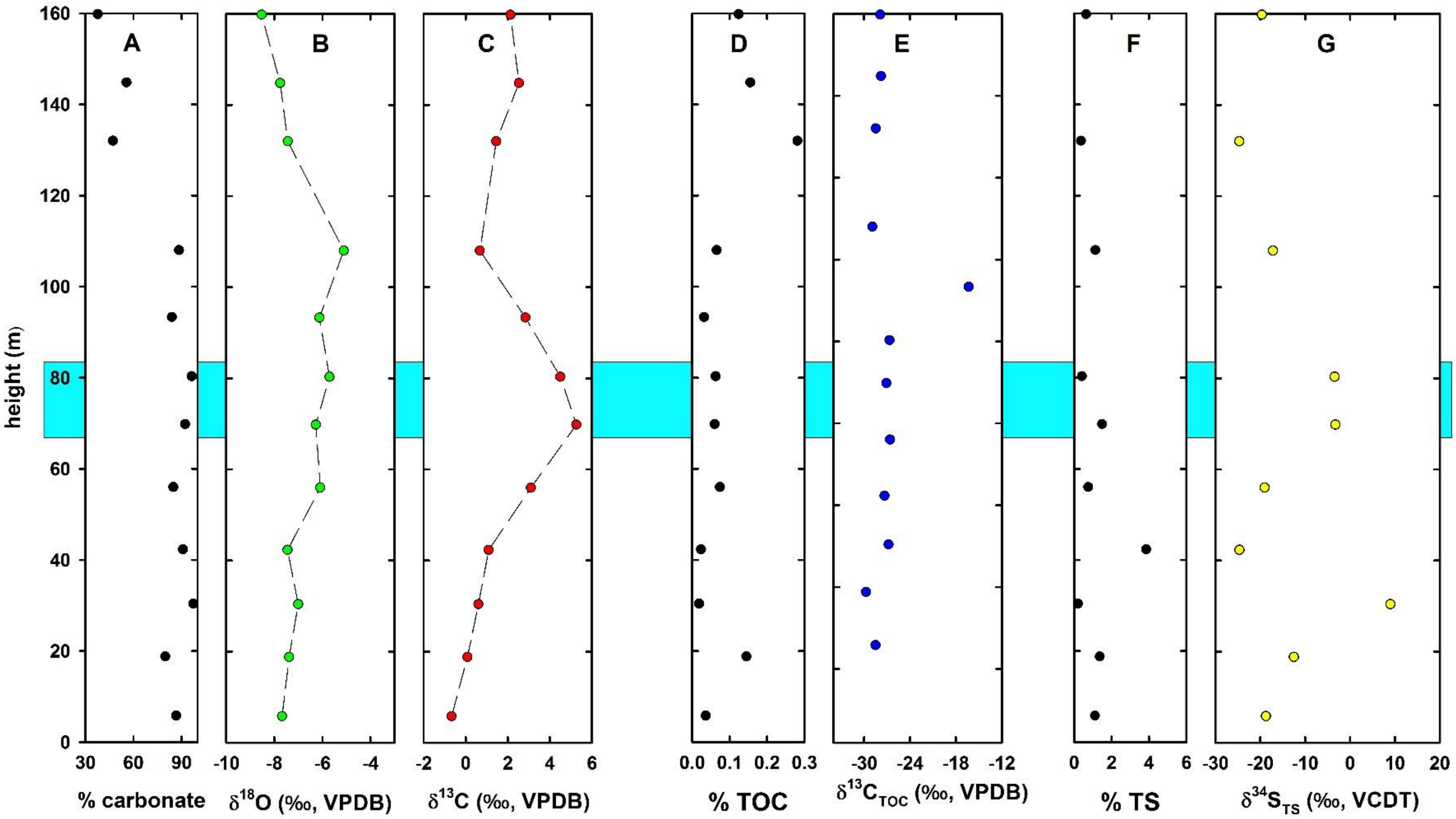

Figure 14: Geochemical Data from Location #2

At Location #1, $\delta^{18}O$ values increase from -10.5‰ at the top of the section to -6.2‰ at the bottom of the section (Figure 13). $\delta^{13}C$ values decrease from about +2.5‰ at the top of the section to about +1.5‰ within 10 meters below the sandstone. Then, they increase within the next 10 m to +3.0‰ at the point I labeled 16.7 m, and decrease after that to +0.6‰ at the bottom of the section. $\delta^{34}S$ values are between -25‰ and -30‰. $\delta^{13}C_{org}$ values are just a little higher, between -23‰ and -29‰.

Table 3: Geochemical Data from Location #2

Location	$\delta^{18}O$	$\delta^{13}C$	$\delta^{13}C_{org}$	$\delta^{34}S$
5.8	-7.68‰	-0.66‰	-28.50‰	-18.70‰
18.8	-7.38‰	0.09‰	-29.74‰	-12.50‰
30.4	-7.00‰	0.61‰	-26.79‰	9.01‰
42.3	-7.44‰	1.10‰	-27.32‰	-24.61‰
56.0	-6.08‰	3.11‰	-26.60‰	-19.02‰
69.8	-6.27‰	5.26‰	-27.08‰	-3.23‰
80.3	-5.70‰	4.50‰	-26.67‰	-3.41‰
93.3	-6.12‰	2.85‰	-16.32‰	
108.0	-5.11‰	0.68‰	-28.90‰	-17.13‰
132.0	-7.44‰	1.46‰	-28.46‰	-24.63‰
144.8	-7.76‰	2.54‰	-27.78‰	
159.8	-8.53‰	2.14‰	-27.89‰	-19.62‰

At Location #2, $\delta^{18}O$ values increase from -8.5‰ at the top of the section to -5.1‰ at the point I labeled 108.0 m (Figure 14). Then, they decrease to -7.7‰ at the bottom of the section. $\delta^{13}C$ values decrease from around +2‰ at the top of the section to a low of +0.7‰ at 108.0 m. Then, they increase to +5.3‰ at 69.8 m. Then, values decrease steeply to +1.1‰ at 42.3 m before a more gentle decrease to -0.7‰ at the bottom of the section. $\delta^{34}S$ values increase from -25‰ at 132.0 m to -3‰ where carbon isotopes peak, and then back down to -25‰ at 42.3 m. $\delta^{13}C_{org}$ values are relatively constant, staying between -26‰ and -30‰ with just one outlier. Raw data is provided in Table 3.

Discussion

The first important goal of this project was to identify the position of the Helderberg Group within the section and locate the Silurian-Devonian boundary. There was no large carbon isotope excursion at Location #1, and the oxygen isotopes also did not match the data obtained by Saltzman (2002). The silicified limestone I observed had not been observed by others at other outcrops of the Helderberg Group. Also, the abundant crinoids in the New Creek Limestone near the Silurian-Devonian boundary were not present. I concluded that the outcrop at Location #1 did not include the Silurian-Devonian boundary, and made additional observations at Location #2 in order to find it.

Location #2 did have the characteristic carbon isotope excursion from +1‰ to over +5‰. The oxygen isotopes matched the pattern observed by Saltzman (2002), decreasing through -6‰ to -8‰. I was unable to make observations of the lithological characteristics of Location #2. I hope future researchers return to this location to make additional, more detailed measurements and observations to more fully characterize the trends I observed.

The location of the Silurian-Devonian boundary and the bulk of the Helderberg Group at Location #2 raised a question about the makeup of the outcrop at Location #1. There was no siltstone beneath the sandstone, where the Shriver Chert should be. Instead, I found a silicified limestone. At the bottom of this silicified limestone was the black chert which should mark the bottom of the Shriver Chert. I concluded that this silicified limestone constituted the Shriver Chert. The silica present silicified the limestone rather than forming the siltstone. This must have also formed in a shallower environment than the rest of the Shriver Chert in order for the shale to be largely absent. A shallower environment would also explain the additional limestone.

The sandstone present in the section has all the characteristics of the Oriskany Sandstone. However, it is overlain by limestone, not shale, as expected. This could indicate either a shallower depositional environment for the Needmore Shale or an interfingering relationship between the Oriskany Sandstone and the Shriver Chert. Interfingering of the Shriver Chert would support the idea of a shallower depositional environment. Rather than a sudden shallowing trend from the siltstone of the Shriver Chert to the Oriskany Sandstone, at this location there is a more gradual, back and forth transition between shallow limestones and the sandstone.

At Location #1 I observed a greater change in oxygen isotopes than carbon isotopes along the section. Oxygen isotopes were probably altered during diagenesis. The fluids present in diagenesis would have altered oxygen much more than carbon because they contain much more oxygen. They probably flowed more easily through the porous sandstone and altered oxygen isotope values less away from the sandstone, explaining the linear trend in oxygen isotopes.

The sulfur isotopes of pyrite show a trend opposite that of the sulfur isotopes measured by others on sulfate. This supports the idea that something other than normal pyrite burial and uncovering was responsible for the trend. If sulfate sulfur in fact became isotopically lighter at this time, pyritic sulfur could only have become heavier if the two processes were not linked, as usual. If pore fluid transport and sediment mixing were poor, indicating a stratified environment, those pore fluids would have resembled a closed environment for sulfate reduction because sulfate replenishment from seawater would also be poor (Rudnicki et al., 2001). In a closed environment, as sulfate levels decrease, the pyrite produced becomes isotopically heavier (Gomes and Hurtgen, 2015). This could explain why sulfate and pyrite are decoupled.

Other factors could also have contributed, though. The amount of fractionation produced by microbial sulfate reduction decreases as the rate of reduction increases (Gomes and Hurtgen, 2015), and an increase in the amount of sulfate available for reduction increases the rate of reduction (Cao et al., 2016). Therefore, a significant increase in the amount of sulfate in the ocean would have caused pyrite to become slightly isotopically heavier anyway. This increase in sulfate could have been caused by the increased weathering suggested by strontium, bulk carbon, and sulfate sulfur isotopes.

Trends in the isotopic composition of organic carbon were also contrary to my expectations. As the isotopic composition of bulk carbon became heavier, the isotopic composition of organic carbon did not change significantly. It seems that these processes were also not linked the way they usually are. A large reservoir of organic carbon in the ocean may have buffered the organic carbon isotopic value of seawater, keeping it stable through this interval (McFadden et al., 2008). An increase in the amount of organic carbon in the ocean also supports increased weathering, and requires the stratified water column suggested by the pyritic sulfur isotopes (McFadden et al., 2008). This large influx of organic carbon would also have done even more to accelerate the rate of sulfate reduction because organic carbon is part of that chemical process (Berner and Raiswell, 1983).

In the future, I hope other researchers will look for the geochemical trends of the Silurian-Devonian boundary at other locations, both on this and other continents. The carbon trend is well-studied, but the trends in both pyritic and sulfate sulfur, and organic carbon, need to be determined elsewhere to find whether they reflect a global phenomenon. Other means of testing the weathering hypothesis should be determined and carried out. I also hope that future researchers continue to explore the excellent outcrops of Corridor H in West Virginia. I am confident they can reveal as much about other intervals as they have revealed about the Helderberg Group and the Silurian-Devonian boundary. It is especially important for someone to return to my Location #2 to make more detailed measurements and observations, and hopefully more precisely correlate those rocks with the rocks of Location #1.

Conclusions

Last year, I hypothesized that the new outcrop of the Helderberg Group would be significantly different from other observed outcrops of the Helderberg Group, reflecting greater variability in lithology than had been previously documented. This hypothesis was confirmed by evidence suggesting a shallower depositional environment for the Shriver Chert at the new location. A relatively sudden transition between siltstone and sandstone observed nearby gives way at the study location to a back and forth transition between limestone and sandstone. Perhaps the basin in which these sediments deposited had other submerged islands of shallower depth than their surroundings. This information could be important for natural gas extraction from the Oriskany Sandstone.

Geochemical trends in the Helderberg Group shed more light on the Silurian-Devonian boundary. Pyritic sulfur and organic carbon isotope trends support the hypothesis that an increase in weathering occurred at the boundary. Strontium and bulk carbon isotope trends already suggested increased weathering. A negative trend in the isotopic composition of sulfate sulfur suggested a change in the isotopic composition of sulfate input into the ocean, which could have been accomplished by weathering of oceanic rocks exposed during a regression. The isotope values of pyritic sulfur may have risen partly due to an increase of sulfate in the ocean, which would have also been a result of increased weathering. Finally, an increase in the amount of organic carbon would explain the lack of change in its isotopic composition, and can also be caused by increased weathering.

The geochemical data also hint at a more stratified ocean during the Silurian-Devonian boundary. The decoupling of pyritic and sulfate sulfur isotope trends can be explained by stratification restricting the amount of sulfate transported into pore fluids. The large amount of organic carbon needed for a stable isotope trend despite the change in bulk carbon would not have been possible if the organic carbon was being oxidized. A large amount of organic carbon in the ocean suggests anoxic conditions, which are present when the water column is stratified.

A regression, an increase in weathering, and stratified oceans begin to explain the cause of the Klonk event at the Silurian-Devonian boundary. These sorts of conditions have caused extinctions at other times, so they could easily have affected life at that time. However, higher resolution sampling is needed to confirm these findings in the central Appalachians, and sampling in other locations must be conducted to determine if these are indeed global phenomena.

Acknowledgements

I must thank both my advisors for the tremendous amount of help they have given me in the course of this project. I must also thank Rebecca Plummer for her assistance with everything related to the mass spectrometer.

Bibliography

Berner, Robert A. and Robert Raiswell. 1983. Burial of organic carbon and pyrite sulfur in sediments over Phanerozoic time: a new theory. *Geochimica et Cosmochimica Acta*, v. 47, p. 855 – 862.

Burke, W. H., R. E. Denison, E. A. Hetherington, R. B. Koepnick, H. F. Nelson, and J. B. Otto. 1982. Variation of seawater $^{87}Sr/^{86}Sr$ throughout Phanerozoic time. *Geology*, v. 10, p. 516 – 519.

Cao, Hansheng, Alan J. Kaufman, Xuanlong Shan, Huan Cui, and Guijie Zhang. 2016. Sulfur isotope constraints on marine transgression in the lacustrine Upper Cretaceous Songliao Basin, northeastern China. *Palaeogeography, Palaeoclimatology, Palaeoecology*, v. 451, p. 152 – 163.

Cohen, K.M., Finney, S.C., Gibbard, P.L. & Fan, J.-X. 2013. The ICS International Chronostratigraphic Chart. Episodes 36: 199-204.

Denkler, Kirk E. and Anita G. Harris. 1988. Conodont-based determination of the Silurian-Devonian boundary in the valley and ridge province, northern and central Appalachians. In *U.S. Geological Survey Bulletin 1837: Shorter Contributions to Paleontology and Stratigraphy*, William J. Sando (ed). United States Government Printing Office: Washington, DC, p. B1 – B13.

Dennison, J. M. 1961. Stratigraphy of Onesquethaw Stage of Devonian in West Virginia and bordering states. *West Virginia Geological Survey Bulletin*, n. 22.

Dorobek, S. L. and J. F. Read. 1986. Sedimentology and basin evolution of the Siluro-Devonian Helderberg Group, central Appalachians. *Journal of Sedimentary Petrology*, v. 56, p. 601 – 613.

Ettensohn, Frank R. and R. Thomas Lierman. 2015. Using black shales to constrain possible tectonic and structural influence on foreland-basin evolution and cratonic yoking: late Taconian Orogeny, Late Ordovician Appalachian Basin, eastern USA. In *Sedimentary Basins and Crustal Processes at Continental Margins: From Modern Hyper-extended Margins to Deformed Ancient Analogues*, G. M. Gibson, F. Roure, and G. Manatschal (eds). Geological Society: London, p. 119 – 141.

Gill, Benjamin C., Timothy W. Lyons, and Matt R. Saltzman. 2007. Parallel, high-resolution carbon and sulfur isotope records of the evolving Paleozoic marine sulfur reservoir. *Palaeogeography, Palaeoclimatology, Palaeoecology*, v. 256, p. 156 – 173.

Gomes, Maya L. and Matthew T. Hurtgen. 2015. Sulfur isotope fractionation in modern euxinic systems: Implications for paleoenvironmental reconstructions of paired sulfate–sulfide isotope records. *Geochimica et Cosmochimica Acta*, v. 157, p. 39 – 55.

Hammarlund, Emma U., Tais W. Dahl, David A. T. Harper, David P. G. Bond, Arne T. Nielsen, Christian J. Bjerrum, Niels H. Schovsbo, Hans P. Schönlaub, Jan A. Zalasiewicz, and Donald E. Canfield. 2012. A sulfidic driver for the end-Ordovician mass extinction. *Earth and Planetary Science Letters*, v. 331 – 332, p. 128 – 139.

Head, James William, III. 1969. An integrated model of carbonate depositional basin evolution; late Cayugan (upper Silurian) and Helderbergian (lower Devonian) of the central Appalachians. Ph.D. dissertation, Brown University.

Jeppsson, Lennart. 1998. Silurian cycles; linkages of dynamic stratigraphy with atmospheric, oceanic, and tectonic changes. *Bulletin - New York State Museum*, v. 491, p. 239 – 257.

Kaufman, Alan J., Stein B. Jacobsen, and Andrew H. Knoll. 1993. The Vendian record of Sr and C isotopic variations in seawater: Implications for tectonics and paleoclimate. *Earth and Planetary Science Letters*, v. 120, p. 409 – 430.

Magaritz, Mordeckai, R. V. Krishnamurthy, and William T. Holser. 1992. Parallel trends in organic and inorganic carbon isotopes across the Permian/Triassic boundary. *American Journal of Science*, v. 292, p. 727 – 739.

Malkowski, Krzysztof and Grzegorz Racki. 2009. A global biogeochemical perturbation across the Silurian-Devonian boundary: ocean-continent-biosphere feedbacks. *Palaeogeography, Palaeoclimatology, Palaeoecology*, v. 276, p. 244 – 254.

McFadden, Kathleen A., Jing Huang, Xuelei Chu, Ganqing Jiang, Alan J. Kaufman, Chuanming Zhou, Xunlai Yuan, and Shuhai Xiao. 2008. Pulsed oxidation and biological evolution in the Ediacaran Doushantuo Formation. *Proceedings of the National Academy of Sciences of the United States of America*, v. 105, p. 3197 – 3202.

Rudnicki, Mark D., Henry Elderfield, and Baruch Spiro. 2001. Fractionation of sulfur isotopes during bacterial sulfate reduction in deep ocean sediments at elevated temperatures. *Geochimica et Cosmochimica Acta*, v. 65, p. 777 – 789.

Saltzman, Matthew R. 2002. Carbon isotope ($\delta^{13}C$) stratigraphy across the Silurian-Devonian transition in North America: evidence for a perturbation of the global carbon cycle. *Palaeogeography, Palaeoclimatology, Palaeoecology*, v. 187, p. 83 – 100.

Saltzman, Matthew R. 2005. Phosphorus, nitrogen, and the redox evolution of the Paleozoic oceans. *Geology*, v. 33, p. 573 – 576.

West Virginia Division of Highways. "Corridor H Route - Forman to Moorefield." Accessed April 14, 2015. http://www.wvcorridorh.com/route/map6.html

Appendix 1

Location	Reaction to Acid	Dunham Classification	Grain Size	Other Notes
18.7a	vigorous	packstone	125 µm – 177 µm	
17.3a	medium	packstone	88 µm – 125 µm	
8.8a	weak	N/A	125 µm – 710 µm	contains much sand, poorly sorted
7.7a	medium	packstone	125 µm – 177 µm	poorly sorted
5.7a	medium	N/A	177 µm – 500 µm	contains much sand, poorly sorted
4.4a	weak	packstone	177 µm – 250 µm	
2.4a	weak	packstone	125 µm – 177 µm	
1.4a	weak	packstone	125 µm – 177 µm	
0.0a	medium	packstone	125 µm – 177 µm	mm-scale dark layers
1.6	weak	packstone	500 µm – 710 µm	significant amount of quartz
2.7	weak	packstone	177 µm – 250 µm	
4.2	medium	packstone	88 µm – 710 µm	poorly sorted
6.0	medium	packstone	125 µm – 177 µm	
7.3	weak	packstone	125 µm – 177 µm	
9.1	medium	packstone	88 µm – 125 µm	
10.8	medium	packstone	88 µm – 125 µm	mm-scale black spots
12.2	vigorous	wackestone	62 µm – 88 µm	
13.8	medium	wackestone	62 µm – 88 µm	
15.5	vigorous	wackestone	88 µm – 125 µm	
16.7	vigorous	wackestone	88 µm – 125 µm	
18.5	vigorous	packstone	88 µm – 125 µm	
20.0	weak	mudstone	88 µm – 125 µm	sand layer
21.5	weak	wackestone	88 µm – 125 µm	
23.1	vigorous	wackestone	62 µm – 88 µm	
25.1	weak	wackestone	62 µm – 88 µm	
26.7	vigorous	wackestone	62 µm – 88 µm	
28.5	vigorous	wackestone	62 µm – >2mm	very fossiliferous
30.3	vigorous	mudstone	62 µm – 88 µm	
31.8	vigorous	mudstone	62 µm – 88 µm	
33.2	vigorous	mudstone	62 µm – 88 µm	faint <1mm thick layers of larger clasts within mudstone
34.9	vigorous	wackestone	62 µm – 88 µm	
36.6	vigorous	mudstone	62 µm – 88 µm	contains pyrite
38.2	vigorous	mudstone	62 µm – 88 µm	
39.5	vigorous	mudstone	62 µm – 88 µm	
41.0	vigorous	mudstone	62 µm – 88 µm	
45.1	vigorous	wackestone	62 µm – 88 µm	
46.3	vigorous	wackestone	62 µm – 88 µm	

Table 4: Descriptions of hand samples from Location #1

Appendix 2

Location	$\delta^{18}O$	$\delta^{13}C$	$\delta^{13}C_{org}$	$\delta^{34}S$
18.7a	-9.61‰	2.55‰		
17.3a	-9.48‰	2.48‰		
7.7a	-10.13‰	2.34‰		
5.7a	-10.40‰	2.28‰		
4.4a	-10.42‰	1.75‰		
2.4a	-10.71‰	1.54‰		
1.4a	-10.64‰	1.77‰		
0.0a	-9.31‰	1.48‰		
0.0a	-9.47‰	0.28‰		
4.2	-10.51‰	2.44‰		
6.0	-10.39‰	2.08‰		
7.3	-10.44‰	1.85‰		
9.1	-9.73‰	2.05‰		
10.8	-10.46‰	2.42‰		
10.8	-9.87‰	2.10‰		
10.8	-10.47‰	2.23‰		
10.8	-10.34‰	2.19‰		
12.2	-9.77‰	2.54‰		
13.8	-9.66‰	2.46‰		
15.5	-9.27‰	2.99‰		
16.7	-9.09‰	3.02‰		
18.5	-9.35‰	2.92‰		
18.5	-5.32‰	4.58‰		
18.5	-9.79‰	2.64‰		
23.1	-7.74‰	2.52‰		
25.1	-7.67‰	1.61‰		
26.7	-7.43‰	2.57‰	-23.15‰	-24.56‰
26.7	-7.59‰	2.39‰		
28.5	-7.34‰	2.48‰		
30.3	-7.09‰	2.14‰		
31.8	-6.86‰	2.00‰		
31.8	-7.08‰	1.99‰		
33.2	-7.15‰	2.02‰		
34.9	-7.03‰	1.78‰	-28.15‰	-29.40‰
36.6	-7.00‰	1.58‰		
38.2	-7.02‰	1.55‰		
39.5	-6.52‰	2.01‰		
41.0	-6.89‰	1.40‰	-29.10‰	-30.42‰
45.1	-7.01‰	0.72‰		
45.1	-6.98‰	0.58‰		
46.3	-6.19‰	0.63‰		

Table 5: Geochemical Data from Location #1